Tidal deformation of neutron stars from microscopic models of nuclear dynamics

Andrea Sabatucci and Omar Benhar
INFN and Dipartimento di Fisica, "Sapienza" Università di Roma, I-00185 Roma, Italy

(Received 17 January 2020; accepted 25 March 2020; published 27 April 2020)

The observation of the gravitational wave signal GW170817, consistent with emission from the inspiral of a binary neutron-star system, provided information on the tidal deformation of the participating stars. The available data may be exploited to constrain the equation of state of dense nuclear matter as well as to shed light on the underlying models describing nuclear dynamics at the microscopic level. In this paper, we compare the experimental results to the predictions of different theoretical models, based on nonrelativistic nuclear many-body theory, the relativistic field-theoretical formalism, and a more phenomenological approach constrained by observed nuclear properties. Although the precision of the available data does not allow to resolve the degeneracy of the models, our analysis shows a distinct sensitivity to the star compactness predicted by the different equations of state, which turns out to be significantly affected by relativistic boost corrections to the nucleon-nucleon potential.

DOI: 10.1103/PhysRevC.101.045807

I. INTRODUCTION

On August 17, 2017, the Advanced LIGO-Virgo detector network made the first observation of the gravitational wave (GW) signal labeled GW170817, consistent with emission from a coalescing binary neutron-star (NS) system [1]. The detection of this signal, and the later observation of electromagnetic radiation by space- and ground-based telescopes [2] arguably marked the dawning of the long anticipated age of gravitational-wave astronomy.

A great deal of effort is being made to exploit the information extracted from event GW170817 to constrain NS properties, most notably the radius, which are, in turn, related to nuclear matter properties encoded in its equation of state (EOS), such as the compressibility module and the symmetry energy, see Ref. [3] and references therein. The new data will also be critical to the progress of nuclear matter theory because they provide an unprecedented opportunity to test microscopic models of nuclear dynamics in the regime of high density and low temperature, which cannot be accessed by terrestrial experiments.

GWs emitted during a binary inspiral are driven by the tidal deformation of the participating stars, which is largely determined by the nuclear matter EOS [4]. However, theoretical studies are often carried out using models of the EOS which are only partially derived from a microscopic description of the dynamics of dense nuclear matter, see, e.g., Ref. [5], or simple phenomenological parametrizations based on the information available from measured nuclear properties, see, e.g., Ref. [6]. Although the results of these analyses provide valuable information, the extension to the case of fully microscopic models, applicable over the whole range of densities relevant to NSs, is needed to fully exploit the potential of GW observations and shed new light on nuclear dynamics. This issue will be all the more important in view of the detection of the GW emitted in the aftermath of the excitation of quasinormal modes [7–9] because the interpretation of the signals will require the understanding of NS properties other than the EOS, see Ref. [10] and references therein.

In this paper, we analyze the tidal deformation predicted by different neutron-star models to highlight the role played by the description of nuclear dynamics at the microscopic level. The widely employed models that will be referred to as APR1 and APR2 [11,12] as well as the model recently proposed by the authors of Ref. [13], Benhar and Lovato, referred to as BL, have been obtained within the framework of nonrelativistic nuclear many-body theory (NMBT), using a nuclear Hamiltonian strongly constrained by the available empirical information on two- and three-nucleon (NNN) systems. The EOS referred to as GM3, on the other hand, has been derived using the formalism of relativistic quantum field theory and the mean-field approximation [14,15]. This scheme will be referred to as relativistic mean-field theory (RMFT). For comparison, we have also included in our paper a more phenomenological EOS, labeled LS, obtained from extrapolation of nuclear properties within the conceptual framework of the liquid drop model [16]. The BL, GM3, and LS models have been also recently compared in a study of neutrino luminosity and gravitational wave emission of protoneutron stars [17].

Our paper does not include results obtained using the dynamical model based on chiral effective field theory (χEFT). While providing an accurate description of the properties of light nuclei, see, e.g., Ref. [18], chiral potentials are derived from a low-momentum expansion. They are, therefore, inherently limited in the ability to describe dense nuclear matter in which nuclear interactions involve large momenta [19]. This problem is highlighted in Ref. [20], whose authors plainly state that using interactions obtained from χ EFT the EOS of neutron matter can be reliably calculated only up to one

to two times the equilibrium density of isospin-symmetric nuclear matter ϱ_0. In view of the fact that the central density of a neutron star of mass $M = 1.4\,M_\odot$ typically exceeds $3\varrho_0$, chiral Hamiltonians do not appear to be best suited for calculations of neutron-star properties.

The main features of the dynamical models of neutron-star matter are summarized in Sec. II, whereas the formalism employed to obtain the tidal deformability is outlined in Sec. III. The numerical results of our work are reported and discussed in Sec. IV. Finally, in Sec. V, we sum up our findings and state the conclusions.

II. MICROSCOPIC MODELS OF THE EQUATION OF STATE

According to NMBT, nuclear matter can be modeled as a collection of pointlike protons and neutrons, whose dynamics are described by the nonrelativistic Hamiltonian,

$$H = \sum_i \frac{p_i^2}{2m} + \sum_{j>i} v_{ij} + \sum_{k>j>i} V_{ijk}, \tag{1}$$

where m and p_i denote the nucleon mass and momentum, respectively, whereas v_{ij} and V_{ijk} describe two- and three-nucleon interactions. The two-nucleon potential, that reduces to Yukawa's one-pion-exchange potential at long distances, is obtained from an accurate fit to the measured properties of the two-nucleon system in both bound and scattering states, whereas the purely phenomenological three-body term V_{ijk} is needed to explain the ground-state energies of the three-nucleon bound states and obtain a reasonable account of the empirical equilibrium properties of isospin-symmetric nuclear matter.

The many-body Schrödinger equation associated with the Hamiltonian of Eq. (1) can be solved exactly, using stochastic quantum Monte Carlo (QMC) techniques for nuclei with mass number A up to 12. The energies of the ground and low-lying excited states turn out to be in remarkably good agreement with the experimental data [21]. In the $A \to \infty$ limit, the QMC method has been applied to treat both pure neutron matter (PNM), see Ref. [21], and, more recently, isospin-symmetric nuclear matter (SNM) [22]. Accurate calculations of the ground-state energy can also be performed using the variational method [11].

In the APR1 model, matter is assumed to consist of neutrons, protons, electrons, and muons in β equilibrium. The baryonic equation of state—constructed combining PNM and SNM results—is obtained from a Hamiltonian comprising the Argonne v_{18} nucleon-nucleon (NN) potential [23] and the Urbana IX (UIX) three-nucleon (NNN) potential [24]. The expectation value of the Hamiltonian in the ground state, described by a trial wave function including correlation effects, is computed using the cluster expansion formalism and chain summation techniques [11].

The APR2 model—in the literature often referred to as APR—is similar to the APR1 but takes into account the relativistic correction arising from the boost of the NN potential to a frame in which the total momentum of the interacting pair is nonvanishing. These corrections are required to use the phenomenological Argonne v_{18} potential—designed to describe interactions between nucleons in their center-of-mass frame—in the locally inertial frame associated with the star.

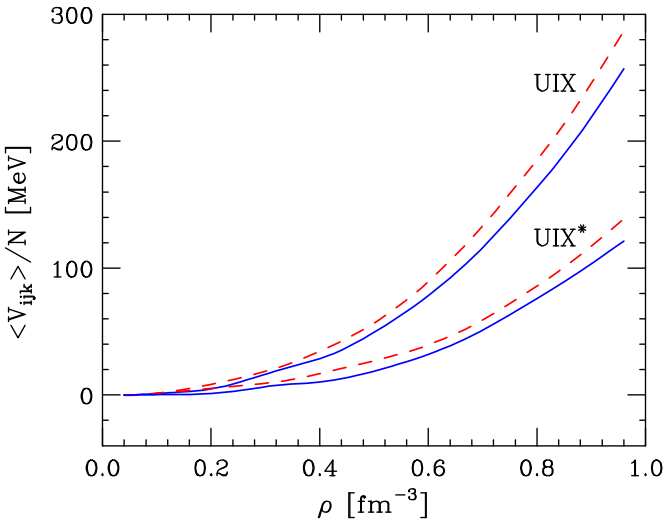

FIG. 1. Ground-state expectation value of the NNN potential per particle, obtained with (UIX*) and without (UIX) inclusion of relativistic boost corrections to the Argonne v_{18} NN potential. The solid and dashed lines correspond to SNM and PNM, respectively.

Inclusion of the boost correction results in the appearance of a sizable repulsive contribution to the potential energy associated with the NN potential and to a corresponding reduction of the repulsion arising from the NNN potential. The modified NNN potential, to be used in conjunction with the boost-corrected Argonne v_{18} NN potential will be referred to as UIX*.

The APR2 EOS of SNM also includes a density-dependent correction to the variational ground-state energy, meant to effectively take into account contributions not included in the calculation. This correction, adjusted to reproduce the empirical saturation properties, reaches a maximum of 4.5 MeV—corresponding to $\approx$30% of the interaction energy—at subnuclear density $\varrho \sim 0.11$ fm^{-3} and rapidly decreases to become negligible in the density region relevant to the NS core.

The impact of the relativistic boost correction on the determination of the potential describing three-nucleon forces is illustrated in Fig. 1. It is apparent that the difference between the potential energy per particle corresponding to the UIX and UIX* interactions begins to be appreciable just above the equilibrium density of SNM $\varrho_0 = 0.16$ fm^{-3} and grows steeply with ϱ.

The large decrease in the repulsion arising from three-nucleon interactions leads to a softening of the EOS, clearly reflected in the density dependence of the pressure of SNM, displayed in Fig. 2. The solid and dashed lines represent the results obtained from the APR2 and APR1 models, respectively. For comparison, the shaded area shows the region consistent with the data obtained from the analysis of nuclear collisions discussed in Ref. [25], providing a constraint on the pressure at $\varrho \geqslant 2\varrho_0$.

The BL model exploits the formalism based on correlated wave functions and the cluster expansion to devise

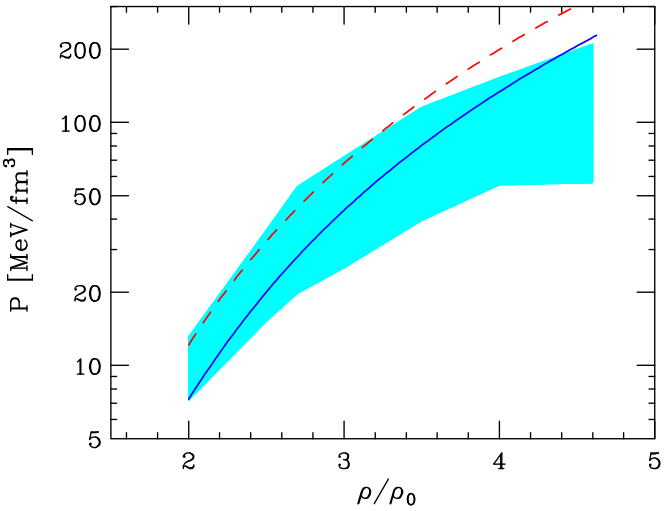

FIG. 2. Density dependence of the pressure of SNM. The solid line corresponds to the APR2 model, including the effect of relativistic boost corrections to the NN potential, whereas the dashed line represents the results of the APR1 model. The shaded area corresponds to the region consistent with the experimental data reported in Ref. [25]. The density is given in units of the equilibrium density $\varrho_0 = 0.16$ fm^{-3}.

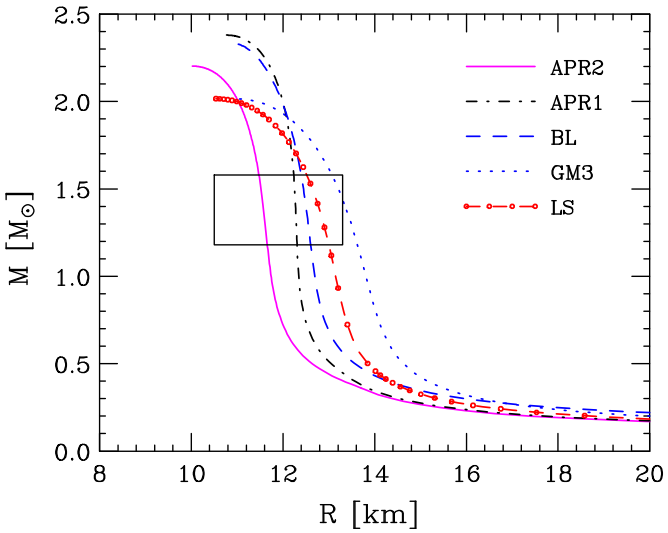

FIG. 3. Mass-radius relations corresponding to the EOSs employed in this paper. The meaning of the labels is explained in Sec. I. The box represents the 90%-confidence-level estimate of mass and radius reported by the LIGO-Virgo Collaborations [34].

an *effective* NN potential, including the effects of two- and three-nucleon forces as well as the density-dependent screening of nuclear interactions arising from strong correlations in coordinate space. This effective potential—obtained from a bare Hamiltonian comprising the Argonne v_6' [26] and UIX potentials—is well behaved and allows to describe the properties of nuclear matter at arbitrary proton fraction using standard perturbation theory and the basis of Fermi gas eigenstates [13].

Within RMFT, nucleons are described as Dirac particles interacting through meson exchange. In the simplest implementation of this scheme, the dynamics are modeled in terms of the scalar-isoscalar field σ, that can be identified with a narrow two-pion resonance and a vector-isoscalar field, the ω meson [27]. In addition, the GM3 model employed in this paper includes the vector-isovector ρ meson [14,15]. The equations of motion obtained from this scheme can only be solved in the mean-field approximation, which amounts to treating the meson fields as classical fields. The nuclear matter EOS can then be obtained in closed form, and the meson masses and coupling constants appearing in the Lagrangian density can be determined by fitting the empirical properties of SNM, that is, the binding energy, equilibrium density, and compressibility.

The models derived within NMBT suffer from the limitations inherent in the nonrelativistic approximation, leading to a violation of causality, determined by the stiffness of the EOS in the $\varrho \to \infty$ limit. On the other hand, RMFT, although being relativistically consistent by construction, is based on a somewhat simplified dynamics and is not constrained by NN data. Moreover, it is plagued by the uncertainty inherent in the use of the mean-field approximation, which is long known to fail in strongly correlated systems [28].

The EOS labeled LS corresponds to the bulk component of the EOS of Lattimer and Swesty [16]. This model, specifically designed for easy implementation in stellar collapse simulations, has been derived from the liquid drop model of the nucleus taking into account the constraints from nuclear phenomenology.

All models considered in our analysis are compatible with the observation of a neutron star of mass $M \gtrsim 2\ M_\odot$ [29], see Fig. 3 below.

III. TIDAL DEFORMATION

A tide is the deformation of a body produced by the gravitational pull of another nearby body. Because the deformation depends on the body's internal structure, the observation of tidal effects in binary neutron-star systems may provide valuable information on the EOS of neutron-star matter.

The orbital motion of two stars gives rise to the emission of GWs that carry away energy and angular momentum. This process leads to a decrease in the orbital radius and, conversely, to an increase in the orbital frequency.

In the early stage of the inspiral, characterized by large orbital separation and low frequency, the two stars—of masses M_1 and M_2 with $M_1 \geqslant M_2$—behave as pointlike bodies, and the evolution of the frequency is primarily determined by the chirp mass $\mathcal{M}$, defined as

$$\mathcal{M} = \frac{(M_1 M_2)^{3/5}}{(M_1 + M_2)^{1/5}}. \tag{2}$$

The details of the internal structure become important as the orbital separation approaches the size of the stars. The tidal field associated with one of the stars induces a mass-quadrupole moment on the companion, which, in turn, generates the same effect on the first star, thus, accelerating coalescence. This effect is quantified by the tidal deformabil-

ity, defined as

$$\Lambda = \frac{2}{3} k_2 \left(\frac{c^2 R}{GM} \right)^5, \tag{3}$$

where M and R are the star's mass and radius, respectively, and k_2 is the second tidal Love number [30]. For any given stellar mass, the radius and the tidal Love number are uniquely determined by the EOS of neutron-star matter.

According to the Newtonian theory of gravity, the effect of a quadrupole tidal field is driven by the *tidal momentum*, defined as

$$\mathcal{E}_{ij} = -\frac{\partial^2 \Phi}{\partial x_i \partial x_j}\bigg|_{\vec{x}=\vec{r}_c}, \tag{4}$$

where Φ is the external gravitational potential. The body subject to the tidal momentum, whose center-of-mass position is specified by the vector $\vec{r}_c$, develops a quadrupole deformation and the associated quadrupole moment,

$$Q_{ij} = \int d^3x \left(x_i x_j - \frac{1}{3}\delta_{ij} r \right) \varrho(\vec{x}), \tag{5}$$

where ϱ is the mass density and r is defined by the equation $r^2 = \delta_{ij} x_i x_j$.

The tensors Q_{ij} and $\mathcal{E}_{ij}$ are both symmetric and traceless. In the weak-field approximation, they are related through

$$Q_{ij} = -\lambda \mathcal{E}_{ij}, \tag{6}$$

and simple dimensional considerations lead to

$$\lambda = \tfrac{2}{3} k_2 R^5 G^{-1}, \tag{7}$$

where the dimensionless constant k_2 is the second tidal Love number of Eq. (3) and $2/3$ is a conventional factor.

The general relativistic treatment of quadrupole deformations of neutron stars involves the study of linearized perturbations of the equilibrium configurations [31]. The metric tensor is written as

$$g_{\alpha\beta} = g^{(0)}_{\alpha\beta} + h_{\alpha\beta}, \tag{8}$$

where

$$g^{(0)}_{\alpha\beta} = \mathrm{diag}(-e^{2\nu(r)}, e^{2\varphi(r)}, r^2, r^2 \sin^2\theta) \tag{9}$$

is the metric of static and spherically symmetric space-time, and the perturbation fulfills the requirement $|h_{\alpha\beta}| \ll 1$.

Quadrupole effects are associated with the $\ell = 2$ even-parity contribution to the expansion of $h_{\alpha\beta}$ in tensorial spherical harmonics, whose radial shape is described by the function $H(r)$, obeying the differential equation [30],

$$H'' + H' \left\{ \frac{2}{r} + e^{2\varphi} \left[\frac{2M(r)}{r^2} + 4\pi r (P - \epsilon) \right] \right\} + H \left[-\frac{6e^{2\varphi}}{r^2} + 4\pi e^{2\varphi} \left(5\epsilon + 9P + \frac{\epsilon + P}{dP/d\epsilon} \right) - (2\nu')^2 \right] = 0. \tag{10}$$

Integration of Eq. (10) and of the Tolman-Oppenheimer-Volkoff (TOV) equations [32,33] allows to determine the second tidal Love number, whose expression can be cast in the form

$$\begin{aligned} k_2 = {} & \tfrac{8}{5} C^5 (1-2C)^2 [2 + 2C(y-1) - y] \\ & \times \{ 2C[6 - 3y + 3C(5y-8)] \\ & + 4C^3 [13 - 11y + C(3y-2) + 2C^2(1+y)] \\ & + 3(1-2C)^2 [2 - y + 2C(y-1)] \log(1-2C) \}^{-1}, \end{aligned} \tag{11}$$

where C and y are defined as

$$C = \frac{M}{R}, \qquad y = R \frac{H'(R)}{H(R)}, \tag{12}$$

with M and R being the star mass and radius, respectively.

Equation (11) shows that given a model of the EOS determining the values of M and R, a calculation of the tidal Love number k_2 requires the knowledge of the functions H and H', obtained from Eq. (10), evaluated at $r = R$.

IV. NUMERICAL RESULTS

The analysis of the GW170817 signal of Ref. [1] allowed a precise determination of the chirp mass, the resulting value being $\mathcal{M} = 1.188^{+0.004}_{-0.002}\, M_\odot$. On the other hand, the estimates of the component masses and their ratio $q = M_2/M_1$ depend on the assumptions made on the NS spins. In this paper, we will consider the results obtained in the "low-spin" scenario in which the NS spin parameter is restricted to values in agreement with galactic binary NS measurements.

The mass-radius relations corresponding to the EOSs employed in our paper are shown in Fig. 3. The box represents the region compatible with the 90%-confidence-level estimates of mass and radius extracted from the analysis of the GW170817 event, yielding $R_1 = R_2 = 11.9 \pm 1.4$ Km, $1.18 \leqslant M_2 \leqslant 1.36\, M_\odot$, and $1.36 \leqslant M_1 \leqslant 1.58\, M_\odot$ [34]. These values have been obtained using the spectral parametrization of the EOS [35]—constrained to support a NS with mass $M \geqslant 1.97\, M_\odot$—at densities $\varrho > \varrho_0/2$ and the Sly EOS of Ref. [36] at lower densities.

Although the accuracy of the available data does not allow to resolve the degeneracy between the results of different models, it clearly appears that the GM3 EOS is only marginally compatible with observations. The curves corresponding to the BL and APR1 EOSs, obtained from NMBT using similar nuclear Hamiltonians, lie close to one another, whereas the differences with respect to the APR2 model show that the relativistic boost correction to the NN potential and the associated modification of the NNN potential result in an appreciable softening of the EOS, see Fig. 2.

The tidal deformability Λ—computed using Eq. (3) with the values of mass and radius obtained from the EOSs described in Sec. II—is displayed in Fig. 4 as a function of the stellar mass. The vertical bar represents the 90%-confidence-level estimate, $70 \leqslant \Lambda(1.4\, M_\odot) \leqslant 580$, obtained by the authors of Ref. [34] by expanding the function $M^5 \Lambda(M)$ around $M = 1.4\, M_\odot$. The emerging pattern, showing that, for any given M, the results obtained from different models are

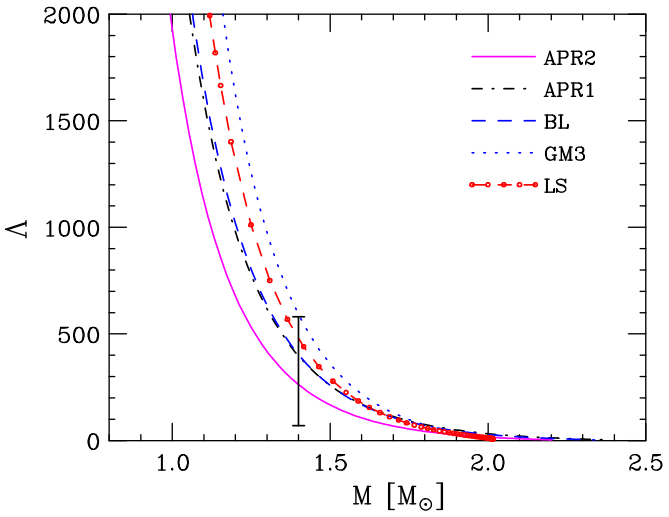

FIG. 4. Tidal deformability obtained from the EOSs described in Sec. II, displayed as a function of the stellar mass. The vertical bar in the lower panel represents the range of Λ for a star of mass $M = 1.4\,M_\odot$, extracted from the analysis of the GW170817 signal [34].

ordered according to the compactness C, see Eq. (12), are consistent with Fig. 3.

The authors of Ref. [1] also report the results of an analysis aimed at pinning down the tidal deformability of the components of the binary system Λ_1 and Λ_2.

Assuming a uniform prior on the quantity,

$$\tilde{\Lambda} = \frac{16}{13}\frac{\left[(M_1 + 12M_2)M_1^4\Lambda_1 + (M_2 + 12M_1)M_2^4\Lambda_2\right]}{(M_1 + M_2)} \quad (13)$$

determining the GW phase, its value in the low-spin scenario has been constrained to $\tilde{\Lambda} \leqslant 800$ at 90% confidence level. The posterior distribution function for Λ_1 and Λ_2 was derived using this constraint and assuming that both stars in the binary system can be described using the same EOS.

In order to compare theoretical predictions to these data, for each EOS, we have generated pairs of stars with masses M_1 and M_2, distributed according to the joint probability distribution reported in Ref. [1] for the low-spin scenario. Because the initial condition for the integration of the TOV equations is the central density ϱ_0, not the mass of the star, we have solved the equations for a wide range of central densities to obtain the function $M(\varrho_0)$. Interpolation of this function in the region in which $dM/d\varrho_0 \geqslant 0$, corresponding to stable equilibrium configurations, yields the values of central density of the stars belonging to the binary system, needed to obtain their radii and tidal deformabilities.

The radii of NSs with masses M_1 and M_2 within the ranges reported by the authors of Ref. [34], obtained using the EOSs described in Sec. II, are listed in Table I.

The results of our calculations of the tidal deformabilities Λ_1 and Λ_2 are displayed in Fig. 5 together with the data resulting from the analysis performed by the LIGO-Virgo Collaborations [1]. The thick curves corresponding to different EOSs are clearly ordered according to compactness and appear to be all compatible with the data at 90% confidence level. However, only those obtained from NMBT fall within the region bounded by the 50%-confidence-level contour. The curve corresponding to the APR1 model is not included in the figure because it turns out to be nearly indistinguishable from that labeled BL.

TABLE I. Radii of NSs with masses in the ranges estimated by the authors of Ref. [34]—$1.36 \leqslant M_1/M_\odot \leqslant 1.58$, and $1.18 \leqslant M_2/M_\odot \leqslant 1.36$—computed using the EOSs considered in this paper. The first and second rows report the radii extracted from the analyses of Refs. [34,37], respectively.

EOS	R_1 (km)	R_2 (km)
[34]	10.50–13.30	10.50–13.30
[37]	11.98–12.88	11.89–12.98
APR1	12.21–12.28	12.28–12.30
APR2	11.46–11.58	11.58–11.70
BL	12.38–12.52	12.52–12.61
GM3	12.90–13.24	13.24–13.43
LS	12.48–12.82	12.82–13.00

V. SUMMARY AND CONCLUSIONS

We have compared the data obtained from the analysis of the GW170817 event, detected by the LIGO-Virgo Collaborations [1,34], to the predictions of different microscopic models of nuclear dynamics, based on NMBT and RMFT. For the sake of completeness, the results of a more phenomenological approach, derived from the liquid-drop model of the nucleus, have been also included in our paper.

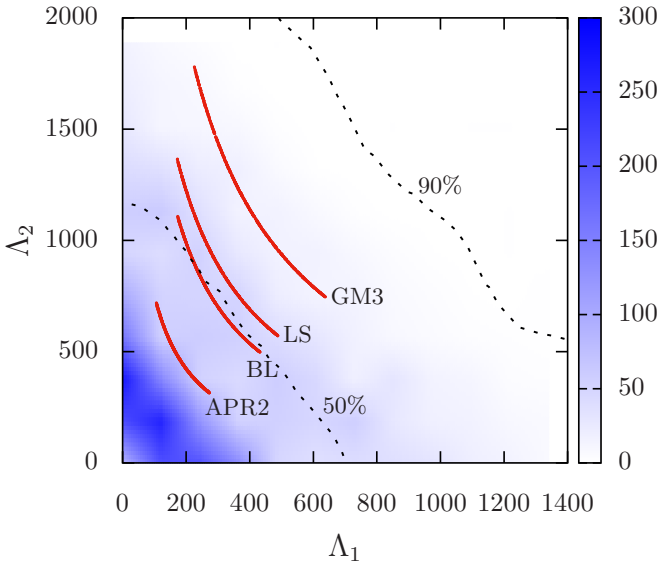

FIG. 5. Probability density of the tidal deformability parameters Λ_1 and Λ_2, obtained from the analysis of the GW170817 signal. The thick solid lines represent the results of calculations carried out using the EOSs described in Sec. II. The dashed lines show the boundaries of the regions enclosing 50% and 90% of the posterior probability density.

The choice to consider matter consisting of nucleons only appears to be reasonable in view of the masses of the coalescing stars, whose values have been estimated to lie in the range of 1.2–1.6 $M_\odot$. In a NS with mass in this range, the density is unlikely to exceed $3\varrho_0$—with ϱ_0 being the equilibrium density of isospin-symmetric nuclear matter—and the transition to more exotic phases, involving strange baryons or deconfined quarks, is not expected to occur.

Even though the precision of the available experimental information does not allow to resolve the degeneracy between the predictions of different models, our analysis shows a distinct sensitivity to the star compactness, whose value is driven by the EOS and the underlying description of nuclear dynamics. Models based on NMBT in which the dynamics is strongly constrained by the properties of the two- and three-nucleon systems, yield similar predictions as shown by a comparison between the results obtained from the APR1 and BL models. However, the inclusion of relativistic boost corrections to the NN potential and the associated modification of the NNN potential result in a softening of the EOS at high density, leading to a sizable change in the mass-radius relation determining the compactness. It is also worth noting that boost corrections push the occurrence of the noncausal behavior of the EOS towards higher density, thus, expanding the range of applicability of the APR2 model of Ref. [12]. On the other hand, a comparison between the results obtained from NMBT and RMFT suggests that the low compactness predicted by the GM3 EOS is likely to be ascribed to the mean-field approximation and to the use of a simplified dynamical model, rather than to relativistic corrections to the potential describing NN interactions.

The possibility to extract more stringent constraints, combining the data collected by the LIGO-Virgo Collaborations with those obtained from observations of bursts in accreting low-mass x-ray binaries, has been recently investigated by the authors of Ref. [37]. Although yielding mass ranges close to those reported by Ref. [34], this analysis—based on a phenomenlogical parametrization of the EOS—sets more stringent bounds on the radii R_1 and R_2, see Table I.

The first observation of GW from a coalescing double NS binary system and the ensuing developments of the multimessenger approach have allowed to obtain valuable new information on the nuclear matter EOS. Although being important in their own right—in that they allow to pin down average properties of dense nuclear matter, such as the compressibility and the symmetry energy—these data have the potential to shed light on the underlying dynamics at the microscopic level. Future observations with improved sensitivity may allow to constrain the NNN potential models in the high-density regime in which interactions involving more than two nucleons become dominant and shed light on the limits of applicability of the nonrelativistic approximation.

ACKNOWLEDGMENTS

This work was supported by the Italian Istituto Nazionale di Fisica Nucleare (INFN) under grant TEONGRAV. The authors are deeply indebted to A. Maselli for his many suggestions and continued advice. Thanks are also due to V. Ferrari and L. Gualtieri for countless illuminating discussions on gravitational waves and neutron stars. Finally, O.B. gratefully acknowledges the hospitality of the Theoretical Physics Department at CERN where this paper has been prepared.

[1] LIGO Scientific Collaboration and Virgo Collaboration, B. P. Abbott *et al.*, Phys. Rev. Lett. **119**, 161101 (2017).
[2] LIGO Scientific Collaboration and Virgo Collaboration, B. P. Abbott *et al.*, Astrophys. J. Lett. **848**, L12 (2017).
[3] L. Baiotti, Prog. Part. Nucl. Phys. **109**, 103714 (2019).
[4] T. Hinderer, B. D. Lackey, R. N. Lang, and J. S. Read, Phys. Rev. D **81**, 123016 (2010).
[5] I. Tews, J. Margueron, and S. Reddy, Phys. Rev. C **98**, 045804 (2018).
[6] P. G. Krastev and B.-A. Li, J. Phys. G: Nucl. Part. Phys. **46**, 074001 (2019).
[7] N. Andersson and K. D. Kokkotas, Mon. Not. R. Astron. Soc. **299**, 1059 (1998).
[8] O. Benhar, E. Berti, and V. Ferrari, Mon. Not. R. Astron. Soc. **310**, 797 (1999).
[9] O. Benhar, V. Ferrari, and L. Gualtieri, Phys. Rev. D **70**, 124015 (2004).
[10] K. Glampedakis and L. Gualtieri, in *The Physics and Astrophysics of Neutron Stars*, edited by L. Rezzolla, P. Pizzochero, D. I. Jones, N. Rea, and I. Vidaña (Springer Nature, Cham, Switzerland, 2018), p. 673.
[11] A. Akmal and V. R. Pandharipande, Phys. Rev. C **56**, 2261 (1997).
[12] A. Akmal, V. R. Pandharipande, and D. G. Ravenhall, Phys. Rev. C **58**, 1804 (1998).
[13] O. Benhar and A. Lovato, Phys. Rev. C **96**, 054301 (2017).
[14] N. K. Glendenning, Astrophys. J. **293**, 470 (1985).
[15] N. K. Glendenning and S. A. Moszkowski, Phys. Rev. Lett. **67**, 2414 (1991).
[16] J. M. Lattimer and F. D. Swesty, Nucl. Phys. A **535**, 331 (1991).
[17] G. Camelio, A. Lovato, L. Gualtieri, O. Benhar, J. A. Pons, and V. Ferrari, Phys. Rev. D **96**, 043015 (2017).
[18] D. Lonardoni, J. Carlson, S. Gandolfi, J. E. Lynn, K. E. Schmidt, A. Schwenk, and X. B. Wang, Phys. Rev. Lett. **120**, 122502 (2018).
[19] O. Benhar, arXiv:1903.11353.
[20] I. Tews, J. Carlson, S. Gandolfi, and S. Reddy, Astrophys. J. **860**, 149 (2018).
[21] J. Carlson, S. Gandolfi, F. Pederiva, S. C. Pieper, R. Schiavilla, K. E. Schmidt, and R. B. Wiringa, Rev. Mod. Phys. **87**, 1067 (2015).
[22] D. Lonardoni, I. Tews, S. Gandolfi, and J. Carlson, arXiv:1912.09411.
[23] R. B. Wiringa, V. G. J. Stoks, and R. Schiavilla, Phys. Rev. C **51**, 38 (1995).

[24] B. S. Pudliner, V. R. Pandharipande, J. Carlson, S. C. Pieper, and R. B. Wiringa, Phys. Rev. C **56**, 1720 (1997).
[25] P. Danielewicz, R. Lacey, and W. G. Lynch, Science **298**, 1592 (2002).
[26] R. B. Wiringa and S. C. Pieper, Phys. Rev. Lett. **89**, 182501 (2002).
[27] J. D. Walecka, Ann. Phys. (NY) **83**, 491 (1974).
[28] L. P. Kadanoff and G. Baym, *Quantum Statistical Mechanics* (Benjamin, New York, 1972).
[29] P. Demorest, T. Pennucci, S. Ransom, M. Roberts, and J. Hessels, Nature (London) **467**, 1081 (2010).
[30] T. Hinderer, Astrophys. J. **677**, 1216 (2008).
[31] K. S. Thorne and A. Campolattaro, Astrophys. J. **149**, 591 (1967).
[32] R. C. Tolman, Phys. Rev. **55**, 364 (1939).
[33] J. R. Oppenheimer and G. M. Volkoff, Phys. Rev. **55**, 374 (1939).
[34] LIGO Scientific Collaboration and Virgo Collaboration, B. P. Abbott *et al.*, Phys. Rev. Lett. **121**, 161101 (2018).
[35] L. Lindblom, Phys, Rev. D **82**, 103011 (2010).
[36] F. Douchin and P. Haensel, Astron. Astrophys. **380**, 151 (2001).
[37] M. Fasano, T. Abdelsalhin, A. Maselli, and V. Ferrari, Phys. Rev. Lett. **123**, 141101 (2019).